HHS Public Access

Author manuscript

Biochim Biophys Acta. Author manuscript; available in PMC 2017 April 10.

Published in final edited form as:

Biochim Biophys Acta. 2017 April ; 1860(4): 438–449. doi:10.1016/j.bbagrm.2017.01.003.

Chromatin Dynamics Regulate Mesenchymal Stem Cell Lineage Specification and Differentiation to Osteogenesis

Hai Wu[1,*], **Jonathan A.R. Gordon**[1,*], **Troy W. Whitfield**[2], **Phillip W.L. Tai**[1], **Andre J. van Wijnen**[3], **Janet L. Stein**[1], **Gary S. Stein**[1], and **Jane B. Lian**[1]

[1]Department of Biochemistry and Vermont Cancer Center, University of Vermont, Burlington, Vermont, United States

[2]Department of Cell and Developmental Biology, University of Massachusetts Medical School, Worcester, Massachusetts, United States

[3]Department of Orthopedic Surgery, Mayo Clinic, Rochester, Minnesota, United States

Abstract

Multipotent mesenchymal stromal cells (MSCs) are critical for regeneration of multiple tissues. Epigenetic mechanisms are fundamental regulators of lineage specification and cell fate, and as such, we addressed the question of which epigenetic modifications characterize the transition of nascent MSCs to a tissue specific MSC-derived phenotype. By profiling the temporal changes of seven histone marks correlated to gene expression during proliferation, early commitment, matrix deposition, and mineralization stages, we identified distinct epigenetic mechanisms that regulate transcriptional programs necessary for tissue-specific phenotype development. Patterns of stage-specific enrichment of histone modifications revealed distinct modes of repression and activation of gene expression that would not be detected using single endpoint analysis. We discovered that at commitment, H3K27me3 is removed from genes that are upregulated and is not acquired on downregulated genes. Additionally, we found that the absence of H3K4me3 modification at promoters defined a subset of osteoblast-specific upregulated genes, indicating acquisition of acetyl modifications drive activation of these genes. Significantly, loss or gain of H3K36me3 was the primary predictor of dynamic changes in temporal gene expression. Using unsupervised pattern discovery analysis the signature of osteogenic-related histone modifications identified novel functional cis regulatory modules associated with enhancer regions that control tissue-specific genes. Our work provides a cornerstone to understand the epigenetic regulation of transcriptional programs that are important for MSC lineage commitment and lineage, as well as insights to facilitate MSC-based therapeutic interventions.

Keywords

mesenchymal stromal cells; osteoblast; ChIP-Seq; gene expression; chromatin; epigenomics; epigenetics

[*]Authors contribute equally to this work.

Disclosures: The authors have nothing to disclose

1. Introduction

Accumulating evidence from genome-wide studies have indicated that histone modifications, chromatin states and tissue-specific transcriptional regulators are inherited from progenitor cells and thus greatly influence phenotypic commitment and cell-specific gene regulation in progeny [1]. Post-translational modifications of histone proteins at lysine, arginine and serine residues dictate the activation or repressive state of a particular gene or genomic region, depending on the presence or absence of acetyl or methyl groups [2]. Several profiling studies examining constitutive histone modifications have demonstrated that chromatin states define genomic context for specific cell lineages [3]. In addition, dynamic changes in histone modifications can influence basal levels of gene expression and regulate expression of specific genes in tissue specification and differentiation programs [4, 5]. However, for many tissues, the exact contribution of specific histone modifications controlling phenotypic gene expression during the stochastic progression of lineage commitment is not currently well understood.

Mesenchymal stromal cells (MSCs) derived from bone marrow are pluripotent progenitor cells that have the capacity to form and regenerate mature connective tissue, however the molecular heterogeneity of these cells is problematic for their wide-spread clinical use [6]. Under normal physiological conditions, growth factor signaling pathways (e.g. BMP/TGF FGF, Wnt) and downstream transcription factors influence decisions of these cells to commit to the formation bone, cartilage, muscle or fat tissue [7]. During aging, these cell fate decisions are compromised resulting in the production of one tissue at the expense of another (e.g. increased adipose with decreased bone). In culture, MSCs can be readily differentiated into adipocytes, myoblasts, chondrocytes and osteoblasts and have also been shown to have capacity to regenerate cardiac muscle and neurons under induced conditions [8]. It is likely that there is a change in the normal underlying epigenetic landscape of the progenitor population and committed phenotypes that are associated with changes in histone modifications. Although MSCs are a widely used model for lineage commitment, unique changes in histone modifications that establish progression from a progenitor to a defined cell lineage has not been extensively defined.

Osteogenesis is a highly regulated program of commitment and differentiation progressing through well-defined phenotypically distinct cell populations from MSCs to the committed osteoprogenitor, mature osteoblasts and the terminally differentiated osteocyte embedded in mineral [9]. This developmental program is recapitulated in vitro as four distinct stages that include the proliferation, commitment, matrix formation and mineralization which are based on gene expression profiles of each subpopulation of osteoblast lineage cells. Previously, epigenetic regulation of bone formation by histone modifications have been identified from studies reporting the actions of HDACs on chromatin during in skeletal development, as well as other histone and chromatin modifying enzymes [10, 11].

In this study, using osteogenesis as a model, we are testing the hypothesis that distinct constitutive and dynamic changes in histone modifications are associated with MSC commitment. We further postulate that the pattern of histone modifications will define distinct mechanisms contributing to repression and activation of genes required for temporal

stages of osteogenesis. Our study utilizes a homogenous cell population bone marrow-derived MSCs induced into committed osteoprogenitors, sequentially differentiated to osteoblasts (OB) and ultimately into osteocytes that are embedded in a developing mineralized matrix during culture. Each of these stages represent a molecular and functionally distinct population of the osteogenic lineage *in* vivo that have defined roles in bone formation [12].

The genome-wide patterns of 7 different histone marks, H3K4me1, H3K4me3, H3K9me3, H3K9acetyl, H3K27me3, H3K27acetyl and H3K36me3 modifications were profiled and combined with profiles of gene expression (RNA-Seq) during MSC differentiation, in order to define patterns of histone modifications that are indicative of gene expression during MSC differentiation. In general, during osteogenic commitment H3K27me3 is removed from genes that are upregulated and are not acquired on genes that are downregulated, suggesting that repression by this mark is not a major contributor to gene regulation during differentiation. Loss or gain of the transcriptional elongation marker, H3K36me3 was associated with dynamic changes in temporal gene expression. In addition, in a subset of osteoblast-related genes we have discovered absence of H3K4me3 signal associated with proximal promoters of upregulated genes, indicating that acquisition of acetyl modifications drives activation of these genes. Using segmentation analysis based on a combination of histone modifications and transcription factor binding, we have defined novel genomic regions that have osteoblast-related regulatory potential throughout the MSC genome. Many of these identified enhancer regions are likely bone-specific as they overlap with previously identified enhancers regulating craniofacial development [13] as well as their proximity to osteoblast-related genes, including the SIBLING gene cluster.

These discoveries and characterization of epigenetic signatures provide novel insight into gene regulatory mechanisms governing MSC commitment and osteogenic differentiation. These findings are relevant to other mesenchymal lineages and developmental processes and have promise of identifying fresh approaches for tissue regeneration and disease intervention.

2. Materials and Methods

2.1. Cell culture

Primary MSCs were isolated from femurs and tibias of 6 – 8 weeks old SMAA-mCherry mice [14], which were kindly provided by Drs I. Kalajzic and D. Rowe. The bone marrow was flushed into ascorbic acid-free MEM-alpha medium (Hyclone, Novato, CA, USA) supplemented with 1x Pen/Strep antibiotics (Invitrogen, Carlsbad, CA, USA). The crude suspension was twice passed through 20 gauge syringes to dissociate cell clumps, followed by hypotonic lysis of erythrocytes. Cells were gently pelleted and resuspended in MSC growth media (ascorbic acid-free α-MEM medium supplemented with 1x Pen/Strep antibiotics and 18% FBS (Hyclone)). Single cell suspension was obtained by filtering resuspended bone marrow cells through 70 μm metal mesh, and then plated at 10 million cells per 10 cm^2 tissue culture plate (Corning Inc., Corning, NY, USA). Bone marrow stromal cells attached to plate surface after 72 hours were kept and cultured for additional 4 days before enriching for SMAA-mCherry positive cells. SMAA-positive MSCs were plated

at 1.5×10^5 cells per 10 cm culture plate for the expansion in the MSC growth media. BMSCs of passage 6 to 10 were used for all the experiments in this study. All animal work was reviewed and approved by UMASS and/or UVM IACUC (protocol number JL-512).

2.2. Flow cytometry

Cell surface markers on isolated MSCs at passage 8 to 10 were determined by flow cytometry on BD FACSCaliburs (BD Biosciences). Briefly, cells were lifted by 0.05% Trypsin-EDTA solution (Invitrogen) and pelleted at 1000 g for 3 minutes, washed thrice with 1x PBS supplemented with 2% FBS (Hyclone) and 10 mM sodium azide (Sigma-Aldrich, St. Louis, MO, USA), incubated with antibody conjugated with FITC for 20 minutes on ice. After antibody incubation, cells were pelleted at 1000 g for 3 minutes and washed thrice with 1x PBS supplemented with 2% FBS (Hyclone) and 10 mM sodium azide (Sigma-Aldrich). Cells were kept in 1x PBS supplemented with 2% FBS (Hyclone) and 5 mM sodium azide (Sigma-Aldrich) before analysis at 4 °C. Antibodies against cell surface markers were: anti-CD11b-FITC, anti-CD45-FITC, anti-Sca-1-FITC, anti-CD29-FITC; proper IgG isotype controls were used to assess background signal. All antibodies were purchased from BioLegend (San Diego, CA, USA) and used at the dilution ratios recommended by manufacturer.

2.3. RNA isolation, quantitative PCR, and RNA-Seq libraries

RNA isolation and quantitative PCR were performed as previously described [15]. RNA-Seq libraries were built with TruSeq RNA Sample Preparation Kit v2 (Illumina, San Diego, CA, USA) following manufacturer's instruction. Four biologically independent RNA-Seq libraries were prepared for each time point during MSC differentiation. All RNA-Seq libraries were pair-end sequenced (PE100) on a HiSeq-1500. Base calls and sequence reads were generated bcl2fastq software (version 1.8.4, Illumina).

2.4. Chromatin immunoprecipitation sequencing (ChIP-Seq)

At day 0, 7, 14, and 21 of differentiation, approximately 5×10^7 MSCs were washed with PBS and then fixed on plate with 1% formaldehyde for 10 minutes at room temperature to crosslink DNA-protein complexes. Chromatin were prepared and sheared as previously described [15]. Sheared chromatin was used for immunoprecipitation with Runx2 antibody (M-70, Santa Cruz), Ctcf (07-729, Millipore, Billerica, MA, USA), Smc1a (A300-055A, Bethyl Laboratories, Montgomery, TX, USA), H3K4me (ab8895, Abcam, Cambridge, MA, USA), H3K4me3 (ab1012, Abcam), H3K9me3 (Ab8898, Abcam), H3K9ac (39137, Active Motif), H3K27me3 (07-449, Millipore), H3K27ac (07-360, Millipore), H3K36me3 (ab9050, Abcam), ap300 (sc-585 X, Santa Cruz) or Ezh2 (A304-196A, Bethyl Laboratories) or immunoglobulin G (IgG) (12-370, Millipore) followed by purification using Protein-G Dynabeads (Invitrogen). ChIP-Seq libraries from immunoprecipitated DNA were constructed as previously described [15]. DNA libraries were sequenced on an Illumina Genome Analyzer II or Illumina HiSeq-1500. Base calls and sequence reads were generated by Illumina CASAVA or bcl2fastq software (version 1.8 and 1.8.4, respectively, Illumina).). Two independent biological repeats of ChIP-Seq libraries were prepared for each time point, and two input libraries were prepared with sonicated DNA for each time point to compensate for possible variation of chromatin structure during MSC differentiation. For

ChIP qPCR, primer sequences corresponding to genomic regions were generated and evaluated by RT-qPCR on an Applied Biosystems Viia 7 thermocycler (Thermo-Fisher). Sequences and genomic locations are listed in supplemental table 1.

2.5. Western blot

Nuclei extracts were prepared from MSCs cells as previously described [15]. The primary antibodies and their dilutions were: mouse anti-Runx2 monoclonal (Clone 8G5, 1:1000 dilution); rabbit anti-H3 3H1 monoclonal (Cell signaling, 1:2000 dilution). HRP-conjugated secondary antibodies were: goat anti-mouse IgG (Santa Cruz, 1:3000 dilution); goat anti-rabbit IgG (Santa Cruz, 1:3000 dilution). HRP activities were analyzed with Western Lightning Plus Kit (PerkinElmer).

2.6. Bioinformatic analysis of ChIP-Seq and RNA-Seq data

At each time point, short sequences from two independent replicates of ChIP-seq and input libraries were combined, and mapped to the mouse genome (assembly mm10) using Bowtie2 (version 2.0.10) [16]. Peaks (genomic regions of statistically significant enrichment of transcription factor binding or histone modifications) and read counts were determined by MACS2 (Model-Based Analysis of ChIP-Seq, version 2.0.10) [17] using default settings with bandwidth set to 250. Peaks with $p \leq 10^{-5}$ were considered significant and included in subsequent analysis. For Runx2, Ctcf, Smc1a, H3K4me1, and H3K4me3, narrow peaks were called by MACS2; for the rest of histone modifications, broad peaks were called. ChIP-seq read densities were obtained by normalizing the read counts of peaks to a total of 1 million reads. Replicate analysis was performed using IDR [18] and calculating Pearson's correlation coefficient between replicate fragment pileups (wigCorrelate) [19]. Peaks passing IDR threshold and a MACS2 p-value of 0.01 on independent replicated were used as a unified peak call and alignments combined for downstream evaluation. A summary of alignments, peaks and replicate data can be found in supplementary table 2. Sequence data and bigwig files were deposited in GEO (Series GSE76074).

Based on known RefSeq genes [20], the mouse genome was segmented into non-overlapping categories including promoter (2 kb upstream of transcription start site (TSS)), exon, intron, TES region (2 kb downstream of transcription start site (TSS)), upstream region (2 to 10 kb upstream of TSS), and intergenic regions. Relative enrichment of histone-associated DNA at gene promoters between time points was defined by calculating fold enrichment (versus input) ($\log_2$ B – $\log_2$ A) for each gene promoter (or associated genomic region) and a t-test was applied to determine significant difference.

Chromatin states were determined by ChromHMM [21] from histone modification tracks and transcription factors Ctcf, Smc1a, and Runx2, with default setting. Initially 15–25 different chromatin states were determened by ChromHMM and 15 states that have reasonable distinguish power of different chromatin states was finally picked.

GO terms were grouped into the downregulated or upregulated specific terms, i.e. those with at least 70% of the matched genes originated from downregulated or upregulated genes. p values were calculated using hypergeometric test and corrected by Benjamini–Hochberg procedure to control false discovery rate.

3. Results

3.1. Stage-dependent dynamics of gene expression during osteoblast commitment from BMSCs

The goal of our study was to define the signature of histone post-translational modifications during the process of osteogenic differentiation in a population of phenotypically homogeneous MSCs. To achieve this objective, we sorted primary bone marrow-derived MSCs expressing a transgenic SMAA-driven mCherry gene [22] (Figure 1A). This population of MSCs were more uniform in their phenotypic characteristics and differentiation potential to all mesenchymal lineages (Figure 1A). MSC enrichment was confirmed by analysis of known phenotypic markers: Sca1 and Cd29 and depletion of typical hematopoietic lineage marker including CD34, Cd11b, and Cd45. These cells were also determined to be enriched in Nestin and CD146, two widely-used markers for MSCs [23] (Figure 1B). To further validate the multipotency of the selected MSC population, the cells were differentiated into osteoblast, chondrocyte, and adipocyte lineages (Figure 1A).

Although several studies have examined gene expression profile of MSCs undergoing osteogenic differentiation, these studies have by and large, used heterogeneous populations of cells with limited differentiation potential. As the SMAA-positive MSCs represent a more homogeneous population of cells with enhanced differentiation potential, we assessed gene expression changes at four developmental timepoints: proliferating MSCs (day 0), early committing MSCs/preosteoblasts (day 7), matrix depositing and maturating osteoblasts (day 14), and mineralizing osteoblasts (day 21). During differentiation the largest number (10,472) of detectable genes (FPKM ≥ 1) were constitutively expressed (Figure 1C). This suggest that during MSC commitment and subsequent osteoblast differentiation, there are a large number of genes that are expressed at a basal unmodified level. At the onset of osteogenic commitment (Day 0), 223 genes were detected as uniquely transcribed (Figure 1C) and included genes indicative of uncommitted mesenchymal cells (serpinb9g, Klra1, Tnfsf9), genes indicative of other MSC-derived lineages (ApoB, Sox11), and genes directly involved in repression of the osteoblast lineage (Mmp3, Bmp7). During progression of differentiation from day 7 to 21, the numbers of uniquely expressed stage-specific transcripts decreased as the mature osteoblast phenotype was established. We interrogated differentially expressed genes over the entire course of phenotype development and found that the mRNA levels of 2919 genes (24.8% of 11792 expressed genes) demonstrated significant changes of more than 2 fold between two time points. The major shift of transcription took place during early commitment from uncommitted MSCs, with 1336 genes demonstrating differential expression. As expected of cells exiting proliferative phase, gene ontology (GO) analysis demonstrated that categories related to cell cycle, DNA replication, and chromatid segregation were associated with genes downregulated from day 0 to day 7 (Figure 1D). In contrast, ontology categories important for mesenchymal osteogenic differentiation, such as Bmps and Fgfrs, were identified from the day 0 to day 7 upregulated gene set (Figure 1D). At the later stages of osteogenesis (days 14 and 21), the total number of differentially expressed genes decreased over time. However, using the upregulated genes which include Mepe, Bglap2/Ocn, and Dmp1 there was a term enrichment of biomineral tissue development, while the downregulated gene set contributed to terms such as myofibril

assembly and embryonic morphogenesis relating to non-osseous tissue formation. Taken together, our data revealed a highly dynamic transcriptome that reflects the phenotypic and functional shift from multipotent BMSCs to lineage-restricted mature osteoblasts.

3.2. Profiling genes expression changes during MSC differentiation

To define an epigenetic signature of MSC commitment, we grouped genes into expression profiles that displayed distinct temporal changes. The patterns of gene expression changes in MSCs were grouped into sixteen distinct expression profiles (Figure 2A). These detailed profiles of differentially expressed (DE) genes fell into several categories: constitutively expressed (group 13), continuously upregulated (groups 11 and 12) and downregulated (groups 14–16) or bimodal expression patterns (groups 1–10) (Figure 2A). Upregulated and downregulated genes were further grouped by relative fold change in gene expression levels. Of the 75 genes that were highly upregulated (> 128 fold) during differentiation (Figure 2B, group 11: up high), the majority were associated with ontology categories related to glycoproteins and ossification/bone development. This finding is consistent with the MSC model recapitulating a normal process of osteogenic differentiation with abundant expression of late-stage osteoblast markers; Ibsp, Bmp3, Dmp1 and Bglap2.

The gene expression profiles related to distinct phases of MSC commitment and maturation are a potential indicator of stage-specific epigenetic changes. Of particular interest were genes classified into bimodal categories which would related to dynamic changes in gene expression, for example genes in group 2 (bimodal l_h_l_h) and group 5 (bimodal l_h_l_l) represent transient signals to induce naïve MSCs to early committed osteoblasts. Ontology terms associated with these groups are extracellular proteins, secretion, and calcium binding and include genes like Bmp6, Wnt9A, Egr1, Il8 and Fosb. Genes that were downregulated during MSC commitment were classified to define potential epigenetic changes as a marker of gene repression, either transient or permanently suppressed and included transcription factors associated with other MSC-derived lineages or loss of proliferative capacity, including Pparg, Fabp2, Twist2, and Mcm2.

3.3. Functional association between epigenetic and transcriptional changes during MSC commitment and osteogenesis

To obtain mechanistic insights into histone modification influencing gene expression during MSC commitment, we examined the global patterns of histone modifications at the genomic locus of profiled genes. We performed ChIP-seq for a panel of 7 specific histone post-translational modifications encompassing methylations and acetylations on lysine residues of histone H3 (Figure 3). Using the profiled gene groups we calculated normalized read coverage across gene bodies and upstream and downstream regions (+/− 2kb) at the defined differentiation time points for each histone modification (Figure 3). For all the profiled groups (up, down and bimodal regulation) H3K4me and H3K4me3 was largely unchanged ($p > 0.05$) throughout the differentiation time course, with the exception of highly upregulated (up high (group 11)) genes which exhibited a noticeable and significant increase ($p < 0.05$) in H3K4me3 signal near the TSS at day 21. In addition, the highly upregulated group demonstrated a stepwise increase in H3K9ac enrichment as a function of differentiation while there was no appreciable change in H3K9ac in the other profile groups.

This result is consistent with the role of H3K9ac as a marker of highly transcribed genes. H3K27ac enrichment profiles revealed that changes in signal intensity were informative to define up and down regulated gene expression. In highly upregulated genes H3K27ac signal increased across the entire gene region during differentiation and in the up medium (group 12) H3K27ac enrichment increased around the TSS and first part of the gene region, reaching a maxima at day 21. In contrast, downregulated genes displayed a decrease in H3K27ac signal near the TSS as a function of differentiation. Bimodal groups displayed slight differences in H3K27ac, however these changes directly correlated with changes in expression during differentiation.

The histone modification most frequently associated with transcription elongation (H3K36me3), showed a modest increase in enrichment across the gene body for highly upregulated genes and showed no discernable changes in signal intensity for upregulated genes. Notably in downregulated genes there was a precipitous drop in H3K36me3 enrichment following day 0. In genes with bimodal expression patterns the patterns of H3K36me3 enrichment showed similar increases or decreases according to level of gene expression. The dynamic changes in H3K36me3 enrichment in bimodal genes would further support that loss of this mark is informative as an indicator of the loss of gene expression.

H3K27me3 enrichment was significantly decreased at highly upregulated and upregulated gene promoters as a function of differentiation ($p < 0.05$). At day 21 both of these groups displayed almost non-existent levels of H3K27me3 enrichment suggesting that this mark is removed prior to maximal gene expression. In downregulated genes there was no significant change ($p > 0.05$) in H3K27me3 enrichment at gene promoters. Although H3K27me3 is a widely established repressor of gene activation, our results indicate that during osteogenesis there is not a substantial gain of H3K27me3 signal to actively repress downregulated genes. Comparing the H3K27me3 and H3K9me3 enrichment patterns, the loss of H3K27me3 near the TSS is indicative of gene activation whereas H3K9me3 accumulation would indicate terminal repression of genes during osteogenesis.

In support of these findings, it was found that the *Dmp1* and *Bmp3* genes displayed histone enrichment patterns indicative of the highly upregulated group (Figure 4A–B). Bmp3 displayed decreasing levels of H3K27me3 and increasing levels of H3K4me3 at the gene promoter (Figure 4B). Consistent with histone profiles of this group (up high, group 11), there was an increase in H3K36me3 enrichment across the Bmp3 gene body coincident with differentiation. Notably there was a slight increase in H3K27ac and a substantial increase in H3K9ac (data not shown) at this gene during differentiation. In comparison, at the Dmp1 gene, (also in group 11) there was little enrichment of H3K4me3 around the TSS or gene body (Figure 4A). Similar to Bmp3 there was a differentiation-dependent increase ($p > 0.05$) in H3K27ac enrichment as well H3K36me3 throughout the gene body. Histone acetylation marks were increasingly enriched as a function of differentiation and increased Dmp1 gene expression (Figure 4A).

At the *Krt19* gene (down medium, group 15) locus, H3K4me3 enrichment near the promoter demonstrated a time-dependent decrease ($p < 0.05$). In addition, H3K27 and H3K9 acetylation, as well as H3K36me3 enrichment were all drastically decreased ($p < 0.05$) at the

Krt19 gene locus (Figure 4C). The pattern of enrichments at the *Krt19* gene is indicative of characteristic changes in histone marks, demarking a histone signature for downregulated genes. Igf2, a gene with bimodal pattern of expression (bimodal l_h_l_l, group 5) demonstrated a characteristic gain of H3K27ac and H3K36me3 coincident with a transient increase in gene expression (Figure 4D). This would suggest that H3K36me3 enrichment at the gene locus is a dynamic and informative histone mark that correlates with transient gene expression. In addition, we observed H3K27ac enrichment at a distal site which appears to precede or parallel increases in gene expression suggesting a role for this site in regulating gene expression.

To further define the underlying regulators contributing to modification of histone proteins adjacent and within differentially expressed genes, we examined the histone modifying enzymes, p300 and Ezh2, for enrichment within defined genomic regions of Dmp1, Krt19 and Igf2 (Figure 4E). The first exon of Dmp1 was found to be occupied by p300, which at day 21 was enriched 4 fold compared to day 0. Similarly, at *Dmp1* 5′ regulatory regions there was a significant increase in p300 enrichment while Ezh2 occupancy remained largely unchanged during differentiation. These enrichment patterns of p300 correlate with increased levels of histone acetylation at these highly expressed genes during differentiation. In contrast, at the *Krt19* gene locus there was a time-dependent decrease in p300 occupancy, again correlating with decreased acetylation found at this gene during osteogenesis. At the bimodal expressed gene *Igf2* there was a transient increase in p300 enrichment, consistent with the acetylation profile within the gene body (Figure 4E), while Ezh2 showed decreasing occupancy as a function of differentiation. These results demonstrate that enzyme complexes regulating the acetylation or methylation of specific histone residues correlate with histone modification patterns at differentiation regulated genes. The actions of theses enzymes at specific gene loci may represent an underlying mechanism responsible for conferring epigenetic marks that define genes marked for expression as a cell becomes committed to a defined lineage. These findings underscore the importance of the dynamic histone signatures for transcriptional regulation.

3.4. Dynamic chromatin states are coupled with osteoblast differentiation

We next sought to define intragenic histone modification patterns that may influence lineage commitment and osteoblast differentiation by defining chromatin states using a hidden Markov model (ChromHMM). This analysis defines recurring combinatorial and spatial patterns of histone modifications and DNA binding [21] that are important to establish both genic and intergenic regulatory regions contributing to lineage specification. We identified cis-regulatory elements, including promoters, enhancers, insulators, and other regulatory elements in the MSC genome that appear as distinct states during the osteogenic program. These comprehensive chromatin states were then further grouped into six general classes of related functional activity which included; transcribed genes, distal cis regulatory modules (CRMs), insulator, promoter, and repressed domains (Figure 5A). The percentage of each state falling into a specific sub-genomic region was determined (Figure 5B). Introns were found to be frequently associated with transcribed states (states1–3) and promoter-associated states (states 10 and 11). Exon regions were associated with several regulatory states (including transcribed, promoter and CRMs) and showed the most variation between day 0

and 7 (Figure 5B, red boxes). This finding suggests that the shift in regulatory activity is associated with gene activation related to cell commitment. The highest enrichment of transcription factors (Ctcf, Smc1a, and Runx2) was observed in states relating to distal CRMs (states 4 – 8 and 12) and insulators (state 9), and surprisingly, not in promoters (state 10–11), suggesting that a large amount of regulatory activity occurs in these genomic elements.

The proportion of the genome devoted to distinct functional activities was determined by calculating relative abundance and genome coverage of specific states (Figure 5C). Transcription elongation (state 1) showed decreases in both relative abundance and genome coverage during osteoblast differentiation, in line with the tapering numbers of differentially expressed genes. There was a continuous increase of CRMs (states 4–8) during differentiation suggesting that establishment of these regions is important to the transcriptional control and/or epigenetic regulation of the osteoblast lineage. The strong active promoter state (state 10) was generally static although the relative abundance increased slightly at day 21, consistent with the observation that the overall numbers of expressed genes remain largely unchanged during osteoblast differentiation (Figure 1B). Low signal regions associated with gene regulatory regions or intergenic regions (states 2 and 15, respectively) displayed an active gain in relative abundance and a significant increase in genome coverage, indicating a transition to transcriptional dormancy in the late stage of the terminal differentiation. In addition, low signal regions (states 2 and 15) covered the majority of the genome during the entire course of differentiation suggesting that a large proportion of epigenetic landscape remains relatively static during osteogenesis.

In order to determine if states associated with enhancer regions were dynamically changing during MSC commitment, strong enhancer (state 4) and CTCF-mediated enhancer (state 8) were compared at day 0 and day 21 (Figure 5D). The majority (78%) of strong enhancer regions remained constant during osteogenesis with very few regions being uniquely attributable to Day 0 or 21 (3% and 19%, repectively). In contrast, CTCF-mediated enhancer regions demonstrated a large number of constitutively marked regions (50%), however there were a significant number of uniquely defined enhancers preceding commitment (18%) and at terminal differentiation (32%) (Figure 5D). This result would suggest that dynamic lineage-specific enhancers are frequently associated with transcriptional regulators/ nuclear organizers such as CTCF. This is consistent with findings suggesting that developmental and specification signals are acquired by remodeling multi-functional epicentres, frequently defined as super-enhancers [24, 25].

3.5. Genome-wide chromatin states define novel regulatory regions controlling osteogenesis

Our segmentation analysis of several histone modifications defined regions of CRMs that were adjacent to differentially regulated genes. In order to define novel CRMs we used previously established enhancers as a reference we examined the VISTA-defined CRM *5430421F17Rik-Fgfr1* located at Chr8:25300000-2560000 [26]. ChromHMM defined multiple CRMs as enriched for active enhancers as reflected in the level of H3K27ac enrichment (figure 6A) and other histone modifications (Figure S6) at these regions. We

identified 11 regions that are potential active enhancers during differentiation, these include novel enhancers and 4 regions that were previously identified (Figure 6A; black bars) [13]. Most changes in distal CRM states are concentrated in or adjacent to the *Fgfr1* locus, with highly distinguishable changes in the regions far upstream to *Fgfr1* including the *5430421F17Rik* locus (Figure 6A, boxed regions). These CRMs are new candidate enhancers that could modulate gene expressions of *Fgfr1*, *5430421F17Rik*, and other neighboring genes.

We examined p300 occupancy, a regulator of H3K27ac, and found a differentiation-dependent gain of enrichment at the VISTA-defined enhancer mm610, but a relative steady state of p300 occupancy at mm612 during osteoblastogenesis (Figure 6B). CRMs encompassing the VISTA-defined enhancers mm610, mm595, and mm919 acquired H3K27ac in a time-dependent manner, while mm612 region showed a slight decrease of H3K27ac enrichment. The differential occupancy of p300 at mm610 and mm612 was in line with the H3K27ac enrichment patterns at the two regions, suggesting that regulatory activity of mm610 but not mm612 was induced during osteoblastogenesis (Figure 6B). To identify possible regulatory targets of mm610, we surveyed the expression level changes of all known RefSeq genes within 1 Mb range of this enhancer. Of the approximately 30 genes in this region, only two genes, *Fgfr1* (a well-known regulator of osteogenesis during development) and *Ppapdc1b* (a less characterized gene with no known osteoblast function*),* exhibited a continuous increase of mRNA expression concomitant with the enrichment changes in H3K27ac and p300 enrichment at mm610 (Figure 6C). This observation suggests that *Fgfr1* and potentially *Ppapdc1b* are regulatory targets of this enhancer region. This observation also supports that our segmentation analysis combining multiple histone enrichment data sets can define potential enhancer regions.

To further understand how chromatin states reflect the expression of genes regulated during osteoblast differentiation, we examined the chromatin states at a cluster of osteogenic genes localized at chromosome 5, spanning from *Sparcl1* to *Pkd2* (Figure 6D). During osteogenesis, the Dspp gene is transcriptionally inactive and at this locus we observed a constitutively repressed region enriched for H3K27me3. In contrast, the transcriptionally active *Spp1* locus is marked by strong active promoter and transcribed states from proliferation to mature osteoblast stages, in line with the constitutive expression of *Spp1* during osteoblast differentiation. At the *Dmp1* locus, we observed the expansion of Runx2-mediated CRMs (black regions in Figure 6D) and active enhancer states that highly correlate with the highly upregulated expression of *Dmp1* during osteoblast differentiation. We observed a large intergenic gene-poor region (Figure 6D; red box) that was enriched in both transcribed and active enhancer states. This region resembles a regulatory region defined as a “super enhancer” [27, 28] that can modulate the expression of genes in this cluster, and would therefore regulate the progression of osteoblast differentiation from MSCs. Taken together, these results suggest a close correlation of chromatin state dynamics with transcriptional regulation of osteogenesis.

4. Discussion

Mesenchymal stromal cells have a molecular identity that is largely defined by epigenetic modifications which maintain a pluripotent phenotype. Relatively unknown are the dynamic changes in histone modifications leading to commitment and establishment of a defined differentiation program. In our study we have used osteogenesis as a model to examine changes in histone modifications regulating global gene expression during the temporal progression of the osteoblast phenotype. We have identified distinct patterns of specific histone modifications that define gene expression changes associated with stages of differentiation.

One of the striking findings of our study is that during progression of osteoblastogenesis, there is a general loss of histone modifications that are typically associated with gene repression. One such modification, H3K27me3 is tightly linked to inactive gene promoters and is regulated by PRC2 complex through enzyme activity of the methyltransferase EZH2. We find most highly expressed genes are marked by H3K27me3 (in addition to H3K4me3) prior to expression, and H3K27me3 is removed from genes resulting in upregulation of expression corresponding to phenotypic commitment. This is consistent with findings that genes co-marked with H3K4me3 and H3K27me3 are poised for expression and are rapidly induced upon commitment, a feature common to several pluripotent cell models [29, 30]. Unlike other bivalency models, we found that H3K27me3 is rarely gained on gene promoters undergoing repression or downregulation. This is a novel finding, as it would suggest that there is not an active mechanism for gene repression in committed osteoblasts, rather gene repression is dictated by a loss of activation marks, such as H3K36me3 and H3K27ac. This loss of H3K27me3 is also consistent with the observed decrease of EZH2 during MSC commitment and differentiation.

Many studies use H3K4me3 as a proxy for gene expression because of the high correlation with active gene promoters. In our study, H3K4me3 at gene promoters was largely unchanged regardless of whether the genes were up- or down-regulated, with the exception of the most highly upregulated genes (> 128 fold) which demonstrated increased enrichment of H3K4me3 upon terminal differentiation. This would suggest that during MSC commitment and osteogenesis H3K4me3 is not a good indicator of gene expression. In contrast to H3K4me3, dynamic changes in gene expression are highly correlated with changes in H3K36me3 enrichment within gene bodies. This is somewhat expected as H3K36me3 is normally associated with transcriptional elongation [31]. However, in our model this mark is a primary predictor of gene activation or repression as well as relative expression levels, as it is most responsive to fine changes in gene expression as indicated by H3K36me3 enrichment or depletion closely mirroring bimodal gene profiles. Although the current understanding is unclear as to whether H3K36me3 precedes transcription or is consequence of transcriptional elongation, our data in MSCs does not differentiate between these two mechanisms, however it is clear that, as many other studies have suggested, H3K36me3 is tightly coupled to changes in gene expression.

A pertinent question regarding H3K36me3 lies in the roles of methyltransferase and demethylase enzymes regulating H3K36 methylation. Several lines of evidence would

suggest that these enzymes have a direct role in the regulation of osteogenesis. For example the WHSC1 gene encodes for a protein with H3K36 methyltransferase activity and is associated with Wolf-Hirschhorn syndrome; a malady characterized by craniofacial abnormalities and dwarfism [32, 33]. In addition, N066 is a bifunctional H3K4/H3K36 demethylase that has been demonstrated to control expression of osterix (SP7) target genes important for osteogenesis [34]. All together and with our findings, this would suggest that H3K36me3 is a driver of gene expression and we conclude that the observed changes in H3K36me3 in the gene body are most indicative of changes in gene expression levels. Evaluation of this modification in skeletal disorders may be an informative strategy for therapeutic interventions.

Several studies have defined the importance of histone acetylation as a regulator of osteogenesis and bone formation, through the modulation of histone deactylases (HDACs) [10, 11]. Consistent with this line of inquiry, we found that H3K27ac enrichment at gene promoters was indicative of genes that were upregulated. In addition, in genes that were most highly upregulated (> 128 fold) during osteogenesis, there was a large increase of H3K27ac signal across promoters and the entire gene body. This result establishes that accumulation of H3K27ac acts to stably maintain a high level of expression of phenotypic genes. Similar to H3K27ac, increased H3K9ac enrichment was also observed in promoter regions and gene bodies of upregulated genes, however these profiles were not as dynamic or indicative of changes in expression.

The role of H3K27ac is not limited to gene expression and is more associated with delineating cis regulatory modules or enhancers. Using a segmentation analysis strategy we identified several thousand potential CRMs that were identified by the presence of multiple histone marks including H3K27ac and H3K4me. These regions were found to be highly dynamic and change in size and location as a consequence of differentiation. CRM regions that demonstrated the most dynamic changes in levels of H3K27ac enrichment were associated with genes that were involved in biomineral tissue development and mesenchymal cell differentiation strongly suggest that these regions may control the expression of genes critical to commitment and differentiation during osteogenesis. Supporting these findings we were able to identify previously defined CRMs proximal to the Fgfr1 gene involved in limb development during embryogenesis [26]. In addition, our segmentation analysis was able to identify several novel CRMs proximal to Fgfr1 that may aid in the dramatic upregulation of Fgfr1 expression in differentiating MSCs. Furthermore, we were able to define numerous potential CRMs near osteoblast-related genes. Specifically, on chromosome 5, within a cluster of osteogenic genes, we identified several distal and intergenic CRMs that likely regulate the temporal expression of these genes during osteogenesis. Further experiments are needed to define functional relevance of these CRMs, however these findings identified novel regulatory regions that may contribute to specific gene function in osteogenesis, embryonic development or pathological disorders.

In summary, our study demonstrates the importance of temporal stages in defining epigenetic events that lead to phenotypic commitment and specific gene expression. ChIP-seq/epigenetic profile studies from individual cell lines are important to define epigenetic changes between two tissues or cell phenotypes, however temporal data from a linear

progression of differentiation provides additional information that would not observed form single time point analysis. Defining signatures of specific histone modifications is a route to understanding epigenetic regulation of the entire program of gene expression during lineage commitment. We have provided new insights into the complexity of coordinated and dynamic changes in histone modifications to support a differentiation program. Our study is the first comprehensive epigenetic signature supporting osteogenesis from MSCs and is relevant to other tissue-specific differentiation programs. This resource of information will be important for defining epigenetic changes contributing to disease states in the skeleton

Supplementary Material

Refer to Web version on PubMed Central for supplementary material.

Acknowledgments

This work is supported by grants R37 DE012528 and R37 DE012528-24S1 to Jane Lian and grant R01 AR039588 to Gary Stein. We thank Dana Frederick and Jennifer Colby for technical support. We are grateful to Ellen Kittler and the Deep-sequencing Core Facility at UMass Medical School and Tim Hunter, Scott Tighe, and Meghann Palermo at the Advance Genomics Technologies Core at University of Vermont for their technical support.

References

1. Zhu J, Adli M, Zou JY, Verstappen G, Coyne M, Zhang X, Durham T, Miri M, Deshpande V, De Jager PL, Bennett DA, Houmard JA, Muoio DM, Onder TT, Camahort R, Cowan CA, Meissner A, Epstein CB, Shoresh N, Bernstein BE. Genome-wide chromatin state transitions associated with developmental and environmental cues. Cell. 2013; 152:642–654. [PubMed: 23333102]
2. Rivera CM, Ren B. Mapping human epigenomes. Cell. 2013; 155:39–55. [PubMed: 24074860]
3. Zhang JA, Mortazavi A, Williams BA, Wold BJ, Rothenberg EV. Dynamic transformations of genome-wide epigenetic marking and transcriptional control establish T cell identity. Cell. 2012; 149:467–482. [PubMed: 22500808]
4. Gifford CA, Ziller MJ, Gu H, Trapnell C, Donaghey J, Tsankov A, Shalek AK, Kelley DR, Shishkin AA, Issner R, Zhang X, Coyne M, Fostel JL, Holmes L, Meldrim J, Guttman M, Epstein C, Park H, Kohlbacher O, Rinn J, Gnirke A, Lander ES, Bernstein BE, Meissner A. Transcriptional and epigenetic dynamics during specification of human embryonic stem cells. Cell. 2013; 153:1149–1163. [PubMed: 23664763]
5. Popova EY, Xu X, DeWan AT, Salzberg AC, Berg A, Hoh J, Zhang SS, Barnstable CJ. Stage and gene specific signatures defined by histones H3K4me2 and H3K27me3 accompany mammalian retina maturation in vivo. PloS one. 2012; 7:e46867. [PubMed: 23056497]
6. Pacini S. Deterministic and stochastic approaches in the clinical application of mesenchymal stromal cells (MSCs). Frontiers in cell and developmental biology. 2014; 2:50. [PubMed: 25364757]
7. Danisovic L, Varga I, Polak S. Growth factors and chondrogenic differentiation of mesenchymal stem cells. Tissue & cell. 2012; 44:69–73. [PubMed: 22185680]
8. Murphy MB, Moncivais K, Caplan AI. Mesenchymal stem cells: environmentally responsive therapeutics for regenerative medicine. Experimental & molecular medicine. 2013; 45:e54. [PubMed: 24232253]
9. Lian JB, Stein GS, Javed A, van Wijnen AJ, Stein JL, Montecino M, Hassan MQ, Gaur T, Lengner CJ, Young DW. Networks and hubs for the transcriptional control of osteoblastogenesis. Rev Endocr Metab Disord. 2006; 7:1–16. [PubMed: 17051438]
10. Bradley EW, Carpio LR, van Wijnen AJ, McGee-Lawrence ME, Westendorf JJ. Histone Deacetylases in Bone Development and Skeletal Disorders. Physiol Rev. 2015; 95:1359–1381. [PubMed: 26378079]

11. Gordon JA, Stein JL, Westendorf JJ, van Wijnen AJ. Chromatin modifiers and histone modifications in bone formation, regeneration, and therapeutic intervention for bone-related disease. Bone. 2015; 81:739–745. [PubMed: 25836763]
12. Javed A, Chen H, Ghori FY. Genetic and transcriptional control of bone formation. Oral and maxillofacial surgery clinics of North America. 2010; 22:283–293. v. [PubMed: 20713262]
13. Attanasio C, Nord AS, Zhu Y, Blow MJ, Li Z, Liberton DK, Morrison H, Plajzer-Frick I, Holt A, Hosseini R, Phouanenavong S, Akiyama JA, Shoukry M, Afzal V, Rubin EM, FitzPatrick DR, Ren B, Hallgrimsson B, Pennacchio LA, Visel A. Fine tuning of craniofacial morphology by distant-acting enhancers. Science (New York, NY). 2013; 342:1241006.
14. Repic D, Torreggiani E, Franceschetti T, Matthews BG, Ivcevic S, Lichtler AC, Grcevic D, Kalajzic I. Utilization of transgenic models in the evaluation of osteogenic differentiation of embryonic stem cells. Connective tissue research. 2013; 54:296–304. [PubMed: 23782451]
15. Wu H, Whitfield TW, Gordon JA, Dobson JR, Tai PW, van Wijnen AJ, Stein JL, Stein GS, Lian JB. Genomic occupancy of Runx2 with global expression profiling identifies a novel dimension to control of osteoblastogenesis. Genome biology. 2014; 15:R52. [PubMed: 24655370]
16. Langmead B, Trapnell C, Pop M, Salzberg S. Ultrafast and memory-efficient alignment of short DNA sequences to the human genome. Genome biology. 2009; 10:R25. [PubMed: 19261174]
17. Zhang Y, Liu T, Meyer CA, Eeckhoute J, Johnson DS, Bernstein BE, Nusbaum C, Myers RM, Brown M, Li W, Liu XS. Model-based analysis of ChIP-Seq (MACS). Genome biology. 2008; 9:R137. [PubMed: 18798982]
18. Li Q, Brown JB, Huang H, Bickel PJ. Measuring reproducibility of high-throughput experiments. 2011:1752–1779.
19. Kent WJ, Zweig AS, Barber G, Hinrichs AS, Karolchik D. BigWig and BigBed: enabling browsing of large distributed datasets. Bioinformatics (Oxford, England). 2010; 26:2204–2207.
20. Pruitt KD, Tatusova T, Maglott DR. NCBI reference sequences (RefSeq): a curated non-redundant sequence database of genomes, transcripts and proteins. Nucleic Acids Research. 2007; 35:D61–D65. [PubMed: 17130148]
21. Ernst J, Kellis M. ChromHMM: automating chromatin-state discovery and characterization. Nature methods. 2012; 9:215–216. [PubMed: 22373907]
22. Kalajzic Z, Li H, Wang LP, Jiang X, Lamothe K, Adams DJ, Aguila HL, Rowe DW, Kalajzic I. Use of an alpha-smooth muscle actin GFP reporter to identify an osteoprogenitor population. Bone. 2008; 43:501–510. [PubMed: 18571490]
23. Roson-Burgo B, Sanchez-Guijo F, Del Canizo C, De Las Rivas J. Transcriptomic portrait of human Mesenchymal Stromal/Stem Cells isolated from bone marrow and placenta. BMC Genomics. 2014; 15:910. [PubMed: 25326687]
24. Adam RC, Yang H, Rockowitz S, Larsen SB, Nikolova M, Oristian DS, Polak L, Kadaja M, Asare A, Zheng D, Fuchs E. Pioneer factors govern super-enhancer dynamics in stem cell plasticity and lineage choice. Nature. 2015; 521:366–370. [PubMed: 25799994]
25. Hnisz D, Schuijers J, Lin CY, Weintraub AS, Abraham BJ, Lee TI, Bradner JE, Young RA. Convergence of developmental and oncogenic signaling pathways at transcriptional super-enhancers. Molecular cell. 2015; 58:362–370. [PubMed: 25801169]
26. Visel A, Minovitsky S, Dubchak I, Pennacchio LA. VISTA Enhancer Browser--a database of tissue-specific human enhancers. Nucleic Acids Res. 2007; 35:D88–92. [PubMed: 17130149]
27. Hnisz D, Abraham BJ, Lee TI, Lau A, Saint-Andre V, Sigova AA, Hoke HA, Young RA. Super-enhancers in the control of cell identity and disease. Cell. 2013; 155:934–947. [PubMed: 24119843]
28. Whyte WA, Orlando DA, Hnisz D, Abraham BJ, Lin CY, Kagey MH, Rahl PB, Lee TI, Young RA. Master transcription factors and mediator establish super-enhancers at key cell identity genes. Cell. 2013; 153:307–319. [PubMed: 23582322]
29. Harikumar A, Meshorer E. Chromatin remodeling and bivalent histone modifications in embryonic stem cells. EMBO reports. 2015; 16:1609–1619. [PubMed: 26553936]
30. Voigt P, Tee WW, Reinberg D. A double take on bivalent promoters. Genes & development. 2013; 27:1318–1338. [PubMed: 23788621]

31. Guenther MG, Levine SS, Boyer LA, Jaenisch R, Young RA. A chromatin landmark and transcription initiation at most promoters in human cells. Cell. 2007; 130:77–88. [PubMed: 17632057]

32. Sukarova-Angelovska E, Kocova M, Sabolich V, Palcevska S, Angelkova N. Phenotypic variations in wolf-hirschhorn syndrome. Balkan journal of medical genetics : BJMG. 2014; 17:23–30. [PubMed: 25741211]

33. Bergemann AD, Cole F, Hirschhorn K. The etiology of Wolf-Hirschhorn syndrome. Trends in genetics : TIG. 2005; 21:188–195. [PubMed: 15734578]

34. Sinha KM, Yasuda H, Zhou X, deCrombrugghe B. Osterix and NO66 histone demethylase control the chromatin of Osterix target genes during osteoblast differentiation. Journal of bone and mineral research : the official journal of the American Society for Bone and Mineral Research. 2014; 29:855–865.

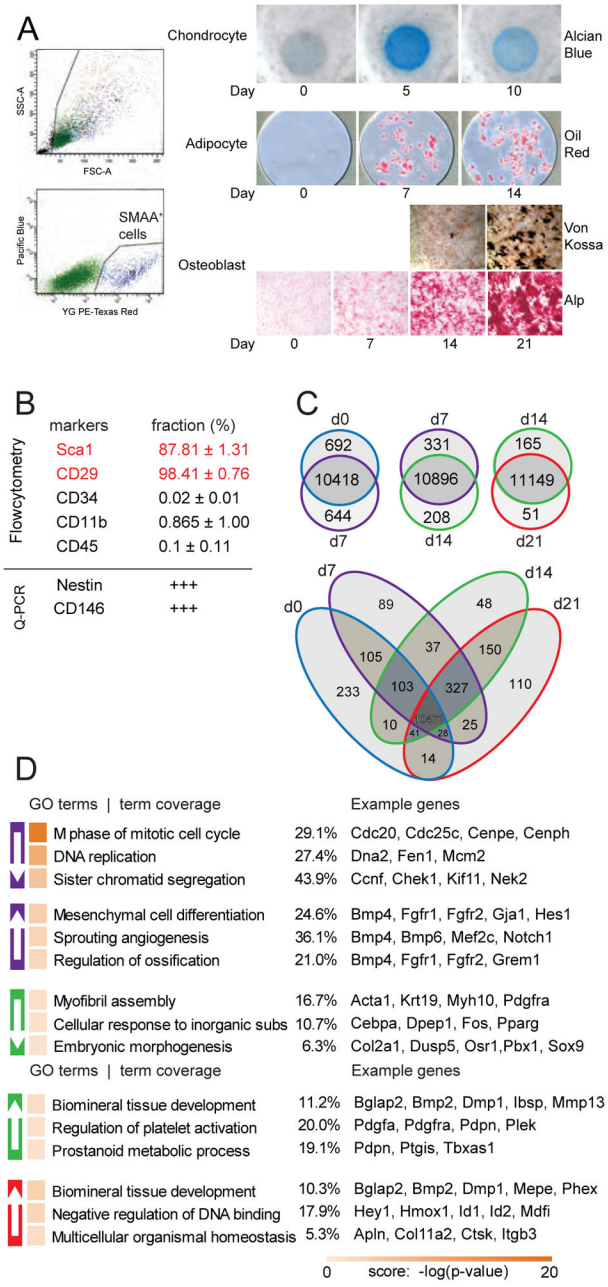

Figure 1. Gene expression dynamics during MSC osteoblast differentiation

A) Primary BMSCs were isolated the diaphyses of tibia and femur of transgenic SMAA-mCherry^{+} mice and sorted by FACS for mCherry expression. Sorted MSCs were induced to chondrogenic, adipogenic and osteoblastic differentiation, and monitored by histological staining for proteoglycan deposition (alcian blue; top panels); lipid deposition (Oil Red O; middle panels); mineral deposition (Von Kossa, lower panels) and Alp activity (bottom panels). B) SMAA+ MSC were characterized for phenotypic markers by flow cytometry or qPCr for gene expression. Values are expressed as fraction of total events (Flow cytometry) or relative expression to bulk MSC population (pPCR). C) Differentially expressed genes

(DE genes) were compared between time points. Numbers of genes downregulated, unchanged, and upregulated at the latter time point are listed from top to bottom. Pair-wise comparisons of all expressed genes (with at least 1 FPKM at one or more time points) during osteoblastic differentiation at indicated time points. Commonly expressed genes (10472) are highlighted in red at the center of the Venn diagram. C) Genes were functionally annotated into GO terms with both downregulated and upregulated genes using the ClueGO package. Enriched GO terms are ranked by score. Term coverage (number of matched genes / total number of genes in a term) and example genes are shown.

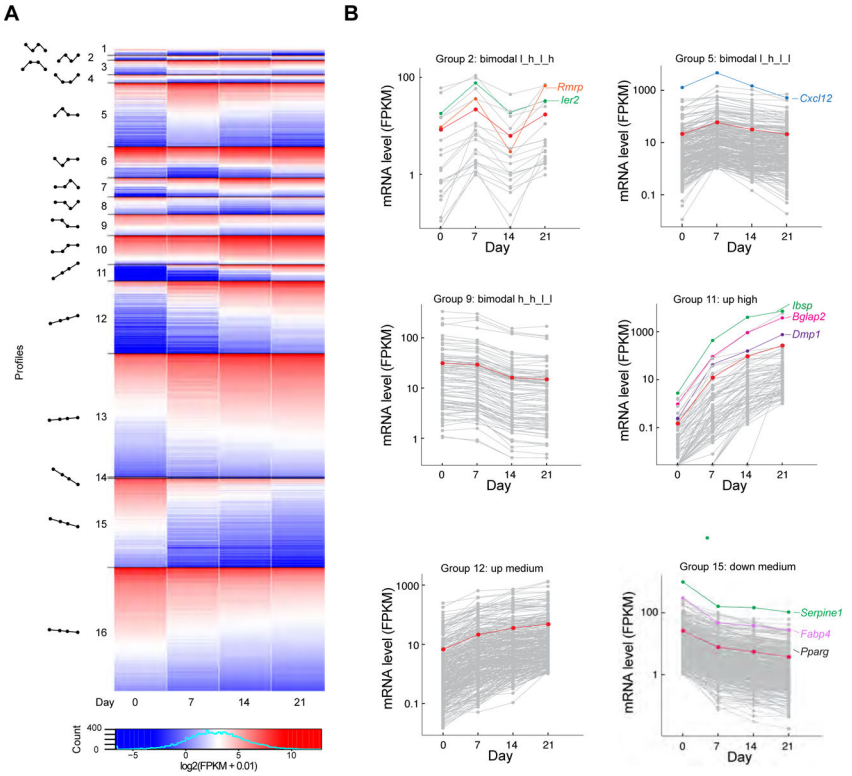

Figure 2. Dynamics of gene expression establishes specific transcription profiles during MSC commitment

A) All significantly expressed genes were grouped into 16 profiles with distinct expression patterns. Schematics of expression patterns and profile numbers are listed adjacent to the heatmap of expression values. B) Detailed expression dynamics of genes within selected groups. Gene names depicted in red represent mean mRNA expression level for genes in these groups and other notable genes are labeled in grey.

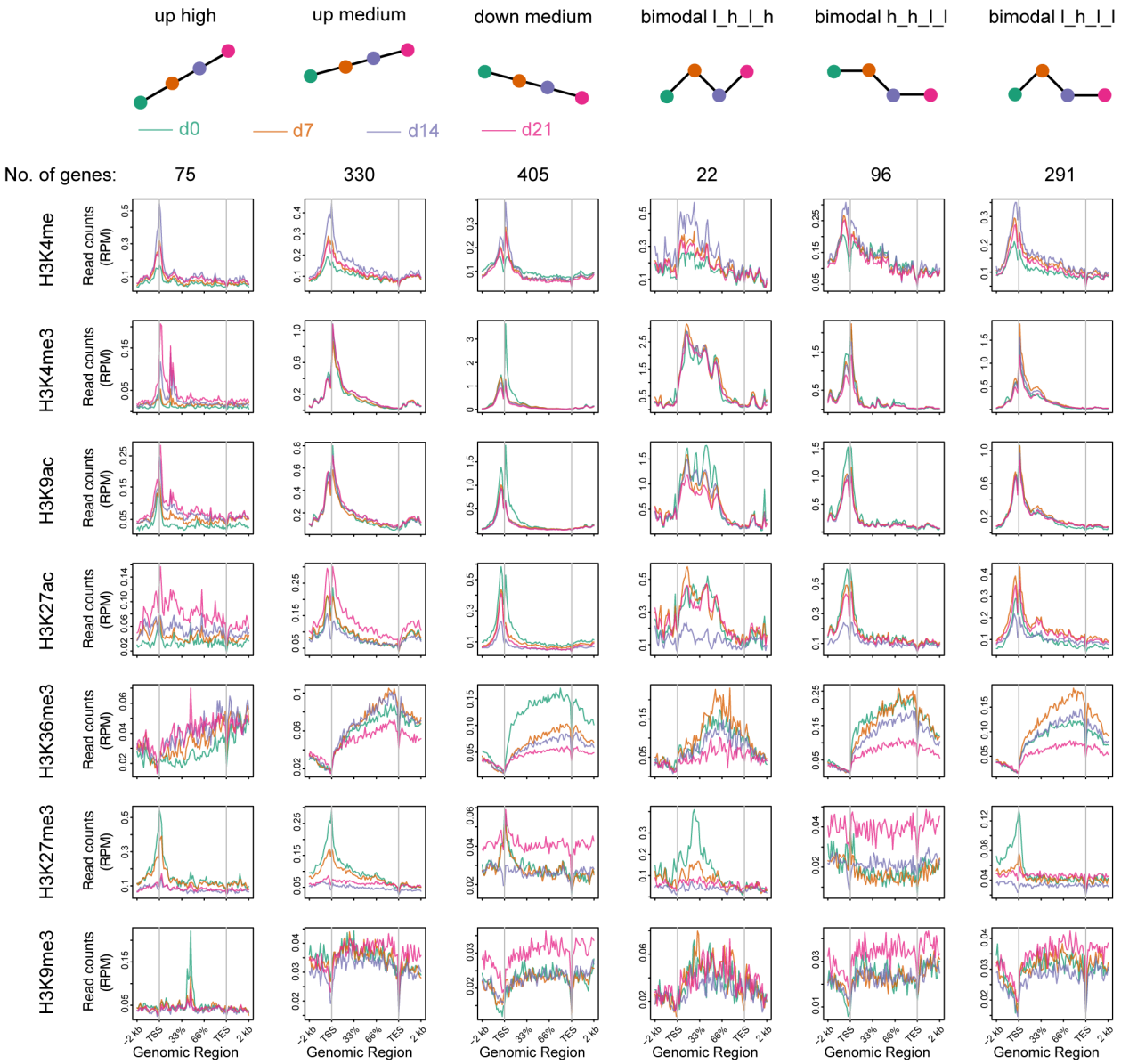

Figure 3. Signatures of histone modifications define transcriptional control during osteoblast differentiation

Aggregation plots of average signal of individual histone modifications (read count per million (RPM)) at gene loci (± 2 kb) at time points during osteoblastic differentiation for each expression profile. Each differentiation time point is defined by a separate color. Signatures are defined by dramatic changes in histone marks. For example, H3K36me3 changes strikingly in genes that are continuously downregulated (down).

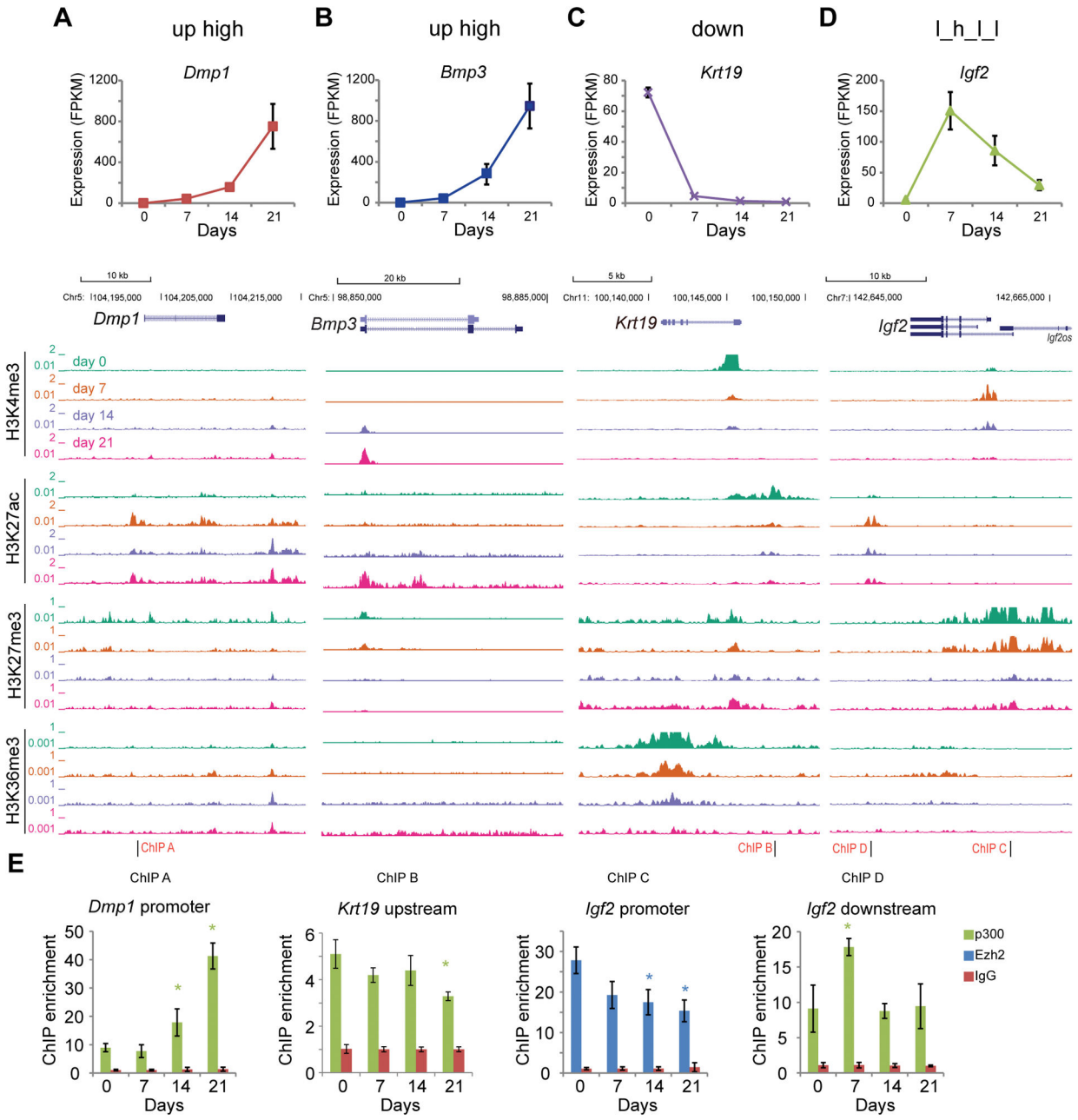

Figure 4. Histone modification signatures are linked to gene expression and the activities of histone modifying enzymes

Expression patterns of genes *Dmp1* from the up high group (A), Bmp3 from the up high group (B), *Krt19* gene in the down group (C), and *Igf2* gene from the bimodal group l_h_l_l (D) had distinct expression patterns during osteoblast differentiation. The enrichment dynamics of four selected histone marks (H3K4me3, H3K27ac, H3K27me3, and H3K36me3) are shown at the loci along with location of primers used in E. **E)** Occupancy of p300 and Ezh2 were evaluated by ChIP-PCR of at selected regions.

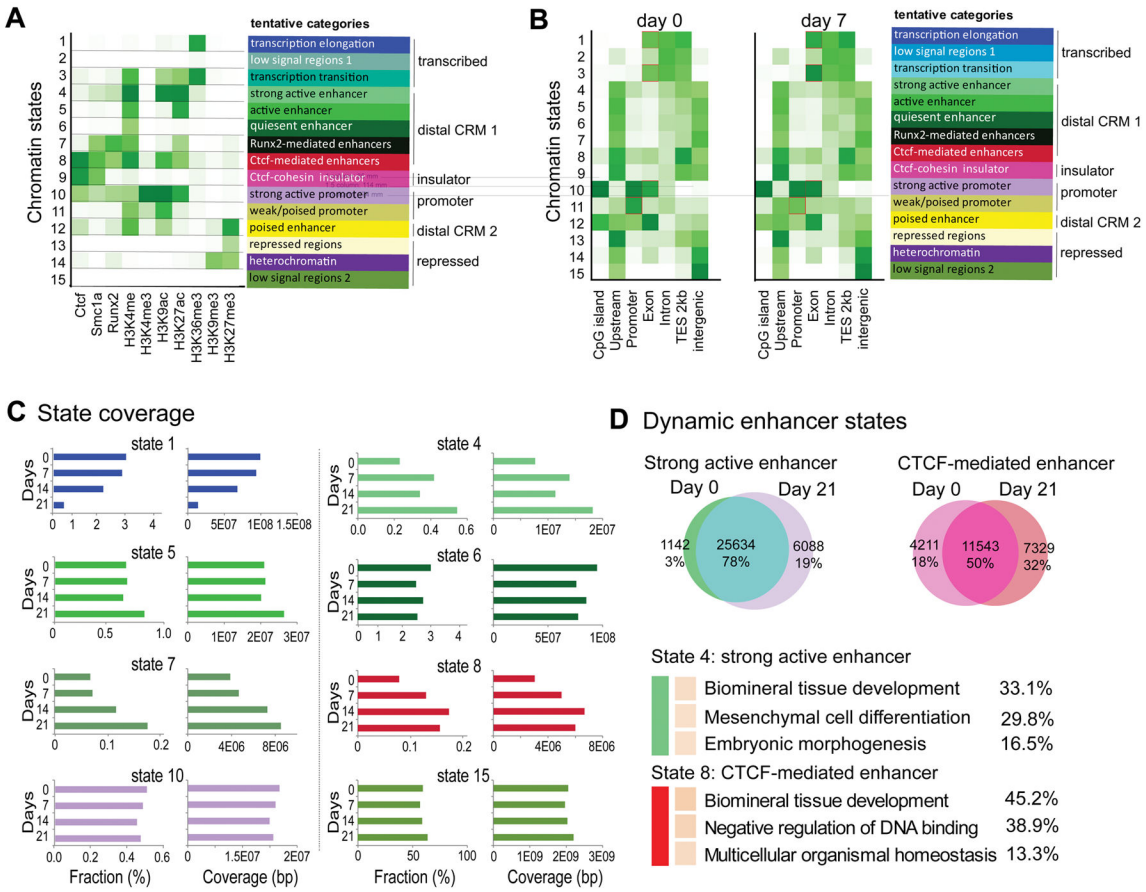

Figure 5. Programmed genome-wide chromatin states during osteoblast differentiation

A) Chromatin states were collectively defined by the combination of multiple marks including transcription factors Ctcf, Smc1a, and Runx2, together with specific histone marks. B) Fold enrichment of chromatin states at different genomic elements at days 0 and 7 of osteoblast differentiation. Several states demonstrating time-dependent alterations in enrichment are highlighted (red). C) The relative abundance (Fraction) in total chromatin states and total genomic coverage (Coverage) of eight functional chromatin states at days 0–21 demark the intrinsic dynamics of the genome over the entire time course of MSC differentiation. D) Venn diagrams depicting dynamic changes in strong-active and CTCF-mediated chromatin states between early and late differentiation stages. Ontology categories associated with dynamically changed enhancers are also shown.

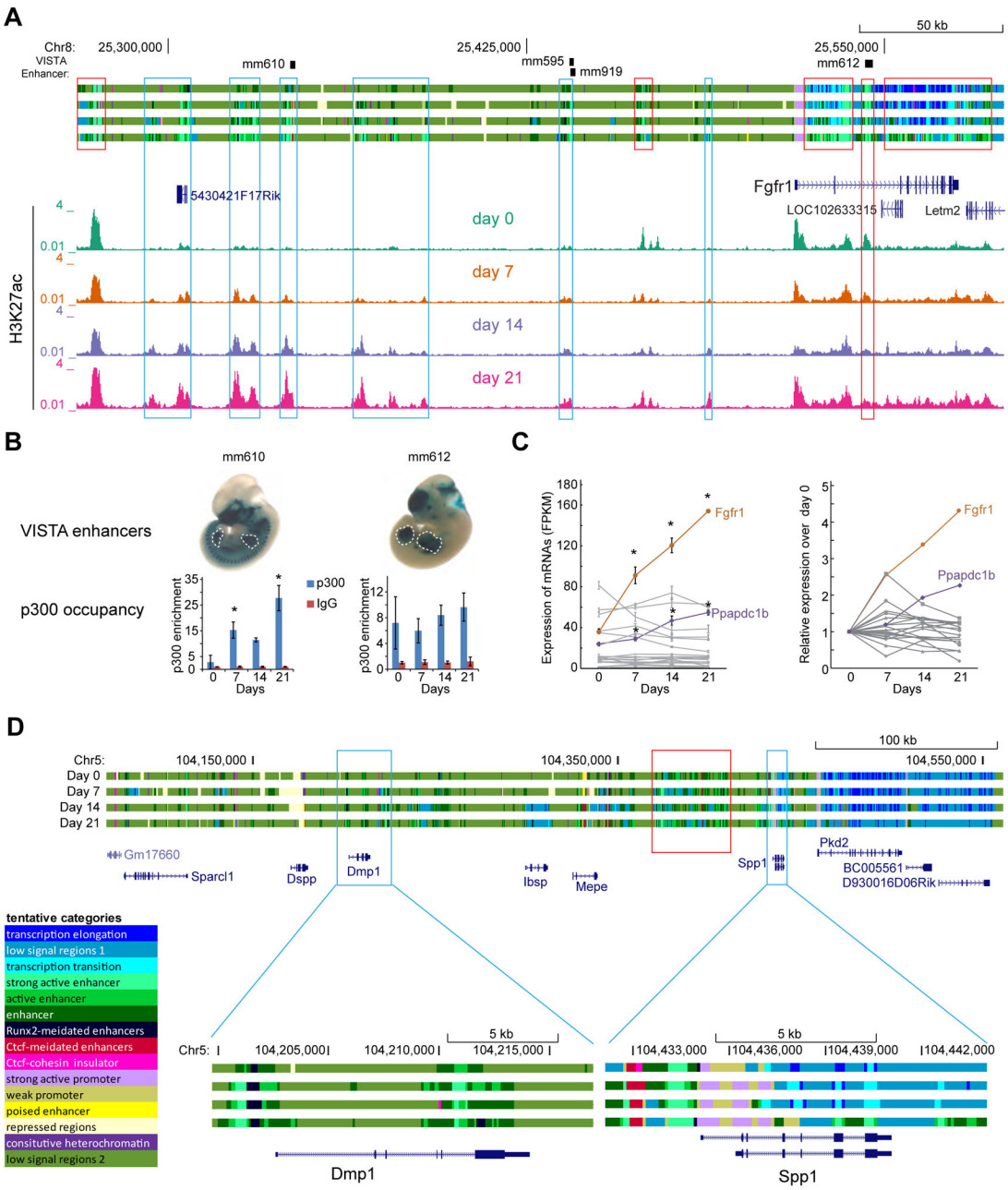

Figure 6. Chromatin states mark the dynamic activities of cis-regulatory modules during MSC commitment to osteoblast

A) Chromatin states indicate dynamic enhancer regions flanking the Fgfr1 gene. Genomic regions identified as osteogenesis specific (gaining H3K27ac during differentiation) are boxed in blue and H3K27ac and constitutive enhancers boxed in red and include annotations for VISTA-identified enhancers that demonstrate tissue-specific expression of beta-galactosidase during embryogenesis [13]. B) p300 occupancy at mm610 and mm612 regions was assessed by ChIP and is consistent with enrichment of H3K27ac at these regions during osteoblast differentiation. * Significant different ($p \leq 0.05$) by t-test. C) Relative expression of genes flanking the 1 Mb regions of Fgfr1 relative to day 0. * Significantly different ($p \leq$

0.05) by two-way ANOVA. D) Chromatin states on chromosome 5 at a gene cluster heavily involved in osteogenesis. Chromatin states in the constitutive active Spp1 and osteogenesis-upregulated Dmp1 were are highlighted (in blue) and demonstrate constitutive and dynamic enhancer acquisition, respectively.